Nanoscale Advances

ROYAL SOCIETY OF CHEMISTRY

COMMUNICATION

View Article Online
View Journal | View Issue

Cite this: *Nanoscale Adv.*, 2023, **5**, 349

Received 7th November 2022
Accepted 30th November 2022

DOI: 10.1039/d2na00782g

rsc.li/nanoscale-advances

Rhenium anchored $Ti_3C_2T_x$ (MXene) nanosheets for electrocatalytic hydrogen production†

Selengesuren Suragtkhuu,[ab] Suvdanchimeg Sunderiya,[a] Solongo Purevdorj,[a] Munkhjargal Bat-Erdene,[c] Batjargal Sainbileg,[d] Michitoshi Hayashi,[d] Abdulaziz S. R. Bati,[e] Joseph G. Shapter,[c] Sarangerel Davaasambuu*[a] and Munkhbayar Batmunkh*[b]

Atomically thin $Ti_3C_2T_x$ (MXene) nanosheets with rich termination groups, acting as active sites for effective functionalization, are used as an efficient solid support to host rhenium (Re) nanoparticles for the electrocatalytic hydrogen evolution reaction (HER). The newly designed electrocatalyst – Re nanoparticles anchored on $Ti_3C_2T_x$ MXene nanosheets ($Re@Ti_3C_2T_x$) – exhibited promising catalytic activity with a low overpotential of 298 mV to achieve a current density of 10 mV cm^{-2}, while displaying excellent stability. In comparison, the pristine $Ti_3C_2T_x$ MXene requires higher overpotential of 584 mV to obtain the same current density. After being stored under ambient conditions for 30 days, $Re@Ti_3C_2T_x$ retained 100% of its initial catalytic activity for the HER, while the pristine $Ti_3C_2T_x$ retained only 74.8% of its initial value. According to our theoretical calculations using density functional theory, dual Re anchored MXene ($Re@Ti_3C_2T_x$) exhibits a near-zero value of Gibbs free energy ($\Delta G_H^* = -0.06$ eV) for the HER, demonstrating that the presence of Re significantly enhances the electrocatalytic activity of MXene nanosheets. This work introduces a facile strategy to develop an effective electrocatalyst for electrocatalytic hydrogen production.

Introduction

Hydrogen (H_2) has received broad attention as part of the future energy solution to help deal with the growing energy storage problems and environmental pollution. H_2 energy has several advantages, including high energy density, zero pollution emission, no greenhouse gas emission, recyclability and others. The key approach to produce H_2 relies strongly on burning fossil fuels and/or biomass feedstock, leading to significant issues associated with the price and environment.[1] Promisingly, the hydrogen evolution reaction (HER) through electrocatalytic reactions is the most economic and environmentally-friendly path to the future energy transition.[2] To reduce the energy consumption and lower the overpotential for water splitting,[3,4] catalysts have been the main subject of interest for the HER. To date, platinum (Pt) is widely known as the best performing catalyst; yet it has limited applicability because of its scarcity and high cost.[5] This has led to increasing efforts focused on developing alternative electrocatalysts to the traditional Pt for the HER.

In this regard, two-dimensional (2D) layered materials with their fascinating chemical and catalytic properties have garnered much attention as an alternative HER catalyst.[3,6,7] The classic examples of 2D electrocatalyst materials include graphene, MoS_2 and black phosphorus, all of which deliver outstanding HER activities with remarkable stabilities.[8,9] As an emerging class of 2D materials, transition metal carbides/nitrides (MXenes) and their derivatives are regarded as promising alternatives to Pt.[10,11] MXenes have a general structural formula of $M_{n+1}X_nT_x$, where M is a transition metal (*e.g.*, Ti, Mo, and Zr), X represents carbon (C) and/or nitrogen (N), and T_x symbolizes the termination groups such as –OH, –F and =O (n = 1, 2, 3 or 4). Mono- or few-layer MXene nanosheets can be obtained from ceramic MAX phases by removing the A element (generally Al), which has a strong bonding with the transition metal through the etching process, followed by gentle exfoliation.[12–14] 2D MXenes have several extraordinary properties, such as high electronic conductivity (up to 10 000 S cm^{-1}), large surface area and strong affinity with water.[15] Despite their recent discovery, MXenes have found applications in different areas including capacitors,[16] batteries,[17,18] solar cells,[19] and catalysis reactions.[20–23]

[a]*Department of Chemistry, Division of Natural Sciences, School of Arts and Sciences, National University of Mongolia, Ulaanbaatar, 14200, Mongolia. E-mail: sarangerel@num.edu.mn*

[b]*Queensland Micro- and Nanotechnology Centre, School of Environment and Science, Griffith University, Nathan, Queensland, 4111, Australia. E-mail: m.batmunkh@griffith.edu.au*

[c]*Australian Institute for Bioengineering and Nanotechnology, The University of Queensland, Brisbane, Queensland, 4072, Australia*

[d]*Center for Condensed Matter Sciences, Center of Atomic Initiative for New Materials, National Taiwan University, Taipei, 106, Taiwan*

[e]*Centre for Organic Photonics & Electronics, School of Chemistry and Molecular Biosciences, The University of Queensland, Brisbane, Queensland, 4072, Australia*

† Electronic supplementary information (ESI) available. See DOI: https://doi.org/10.1039/d2na00782g

In general, anchoring single metal atoms and/or metallic nanoparticles on a solid support such as graphene and MXenes not only enhances the catalytic activity of electrocatalysts, but also enables reduction of the catalyst costs.[24] Of particular importance in this research area is the functionalities of the support materials. Indeed, the rich termination groups of MXene nanosheets have opened vital avenues for research in designing 2D functional materials for various applications including the electrocatalytic HER. For instance, Zhang *et al.* developed an efficient catalyst using single platinum atoms immobilized on 2D MXene nanosheets for the HER.[25] This novel catalyst displayed an impressive catalytic activity with a low overpotential of 77 mV to achieve 100 mA cm^{-2}, while showing about 40 times greater mass activity than the commercial Pt@C catalyst. Recently, Bat-Erdene *et al.*[22] designed boron-doped MXenes with highly dispersed ruthenium (Ru) nanoparticles (Ru@B-$Ti_3C_2T_x$), exhibiting outstanding catalytic activity for the HER with a low overpotential of 62.9 mV to reach 10 mA cm^{-2} in acidic media. Despite these excellent efforts, the search for novel HER electrocatalysts is still an active area of research, while the availability of many other low-cost metal based materials provide great opportunities to advance this field.[26,27] In this regard, rhenium (Re) has recently attracted increasing attention as a promising catalyst for the HER due to several reasons. Re exhibits an optimal binding energy for adsorption and desorption of protons as well as an excellent exchange current density (comparable to Pt) for the HER.[26,28] It is also about an order of magnitude less expensive than Pt (1/10 the price of Pt and 3/10 the price of Ru). Moreover, Re has great potential to overcome the shortcomings of Pt, and thus deserves exploration for the catalytic HER. Importantly, it was reported that the bulk state of metallic Re is not an appealing candidate for the HER and therefore recommended to downsize it to a nanostructure or more.[29]

Herein, we prepared Re ultrasmall nanoparticles (1–3 nm in diameter) uniformly anchored onto $Ti_3C_2T_x$ (MXene) nanosheets and explored their electrocatalytic activity for the HER in acidic media. In addition to the excellent cycling stability, the newly developed electrocatalyst (Re@$Ti_3C_2T_x$) displayed promising catalytic activity for the HER with an overpotential of 298 mV to achieve 10 mA cm^{-2}, which is significantly better than that of the pure MXene. A combination of theoretical calculations and experimental analysis was used to understand the catalytic kinetics of Re anchored onto MXenes.

Results and discussion

The as-prepared $Ti_3C_2T_x$ dispersion was characterized using UV-vis spectroscopy. As shown in Fig. 1a, three characteristic peaks of $Ti_3C_2T_x$ can be observed at 260, 330 and 800 nm wavelengths, showing excellent consistency with previous studies.[22,30,31] The crystallographic structure of the $Ti_3C_2T_x$ flakes was studied by X-ray diffraction (XRD) analysis. As illustrated in Fig. 1b, two main peaks appearing at around 6.5° and 20.7° can be assigned to the (002) and (004), respectively.[22,30,31] Two main changes were observed after etching and exfoliating the MAX phase. First, no residual peak of Ti_3AlC_2 (104) was seen in the $Ti_3C_2T_x$ sample (Fig. S1†). Secondly, the (002) peak shifted from 9.61° to 6.5° due to the increase in *d*-spacing, suggesting the successful synthesis of $Ti_3C_2T_x$ surface termination groups.[31,32]

X-ray photoelectron spectroscopy (XPS) was carried out to determine the chemical and electronic states of $Ti_3C_2T_x$. As depicted in Fig. 1c, the XPS survey scan of $Ti_3C_2T_x$ revealed the presence of all the expected elements, namely Ti, C, O, and F,

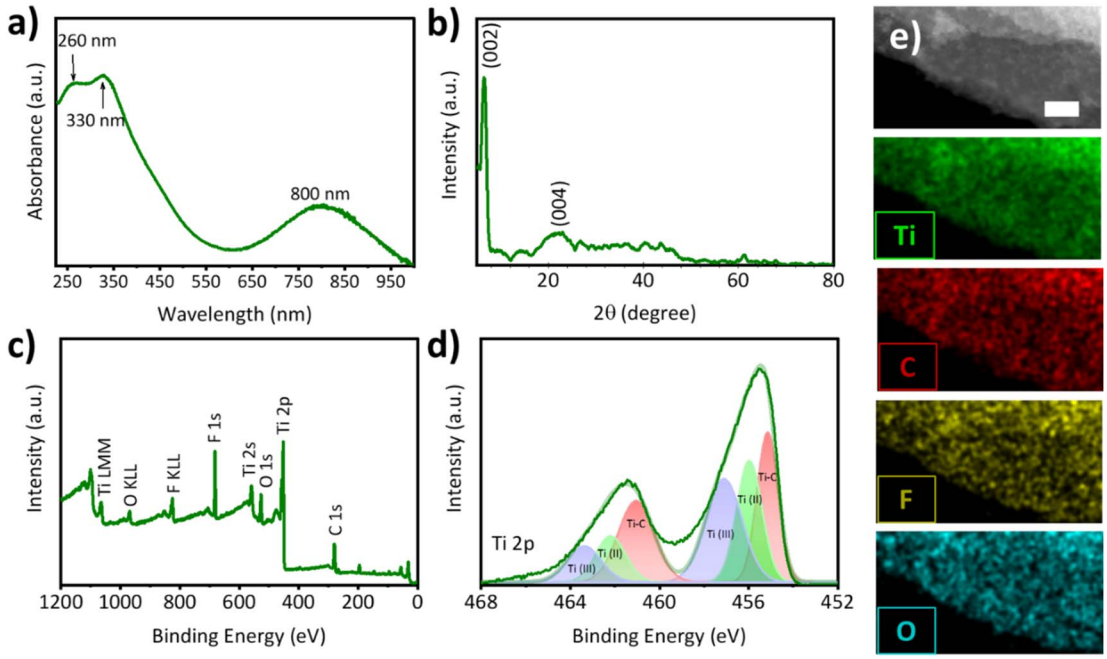

Fig. 1 (a) UV-vis spectrum, (b) XRD pattern, (c) XPS survey scan, (d) HR Ti 2p and (e) HAADF-STEM image (scale bar: 20 nm) and the corresponding EDX elemental (Ti, C, F and O) mapping images of the obtained $Ti_3C_2T_x$ flakes.

further confirming the successful preparation of $Ti_3C_2T_x$. The appearance of F with high intensity suggests the successful introduction of rich termination groups on the surface of $Ti_3C_2T_x$, which is in agreement with the XRD result. Fig. 1d shows the high resolution (HR) Ti 2p spectrum of the as-prepared $Ti_3C_2T_x$, confirming the two asymmetric peaks typically observed in the fresh MXene.[31] In addition to the strong Ti–C bonding (see the HR C 1s spectrum in Fig. S2†), the absence of a peak at around 459 eV binding energy suggests that the $Ti_3C_2T_x$ sample is not oxidized and further confirms the successful preparation of high quality $Ti_3C_2T_x$ flakes. Fig. 1e depicts the high-angle annular dark-field scanning transmission electron microscope (HAADF-STEM) and energy dispersive X-ray (EDX) elemental mapping images of the $Ti_3C_2T_x$ nanosheets. The presence of Ti, C, F and O with highly uniform dispersion suggests that $Ti_3C_2T_x$ flakes with rich O- and F-containing termination groups were successfully prepared.

Further, the as-prepared $Ti_3C_2T_x$ flakes were mixed with Re_2O_7 at a ratio of 4 : 1 (wt%). After freeze-drying, the mixture was annealed at 500 °C for 3 h in a quartz tube under an Ar gas flow. During the annealing process, Re_2O_7 is thermally reduced to Re nanoparticles, anchoring uniformly on the surface of MXene. First, XRD was used to analyze the crystal structure of our Re@$Ti_3C_2T_x$ as presented in Fig. 2a. It can be seen that the XRD pattern of Re@$Ti_3C_2T_x$ was similar to that of $Ti_3C_2T_x$ ((002) and (004 peaks)), suggesting that the introduction of Re nanoparticles did not alter the crystal structure of the MXene. Interestingly, two new characteristic peaks at 37.2° and 53.8° were observed and can be assigned to the (100) peak of Re and (210) peak of ReO_3, respectively.[29,33] Then, XPS was employed to analyze the chemical bond formation of our Re@$Ti_3C_2T_x$. In Fig. 2b, the XPS survey scan of Re@$Ti_3C_2T_x$ shows the existence of Ti, C, O, F and Re confirming the successful synthesis of Re@$Ti_3C_2T_x$. To analyze the oxidation states of Re based on the binding energies HR XPS scans were recorded (see Fig. 2c). The dominant peaks at 41.7 eV and 44.1 eV correspond to the fully reduced Re (0) species, while the peaks at 45.8 eV and 48.2 eV correspond to the oxidized species of Re (ReO_3). The estimated percentages of Re (0) and ReO_3 from high-resolution 4f Re spectra (Fig. 2c) were 48.7% and 51.3%, respectively, in the sample.

The spin–orbit split doublets with a splitting of 2.4 eV for Re were highly consistent with the XPS handbook. These results are not only consistent with previous literature,[29,33,34] but also in excellent agreement with our XRD analysis. Notably, recent work showed that a combination of metallic and partially oxidized Ru nanoparticles is beneficial for overall water splitting reactions including the HER.[35] Therefore, it is reasonable to expect that the presence of both metallic and oxidized Re would be valuable to enhance the catalytic activity of the catalyst.

Fig. 2d and e show the HR transmission electron microscopy (HRTEM) image of Re@$Ti_3C_2T_x$. Two lattice fringe values of 0.32 nm and 0.26 nm can be measured from the HRTEM. While the lattice fringe of 0.26 nm is consistent with previous studies,[36] the spacing of 0.32 nm is slightly higher than that of the typical $Ti_3C_2T_x$, suggesting that the introduction of Re species may be responsible for this enlargement of lattice spacing.[37] Moreover, it can be clearly observed from Fig. 2d that

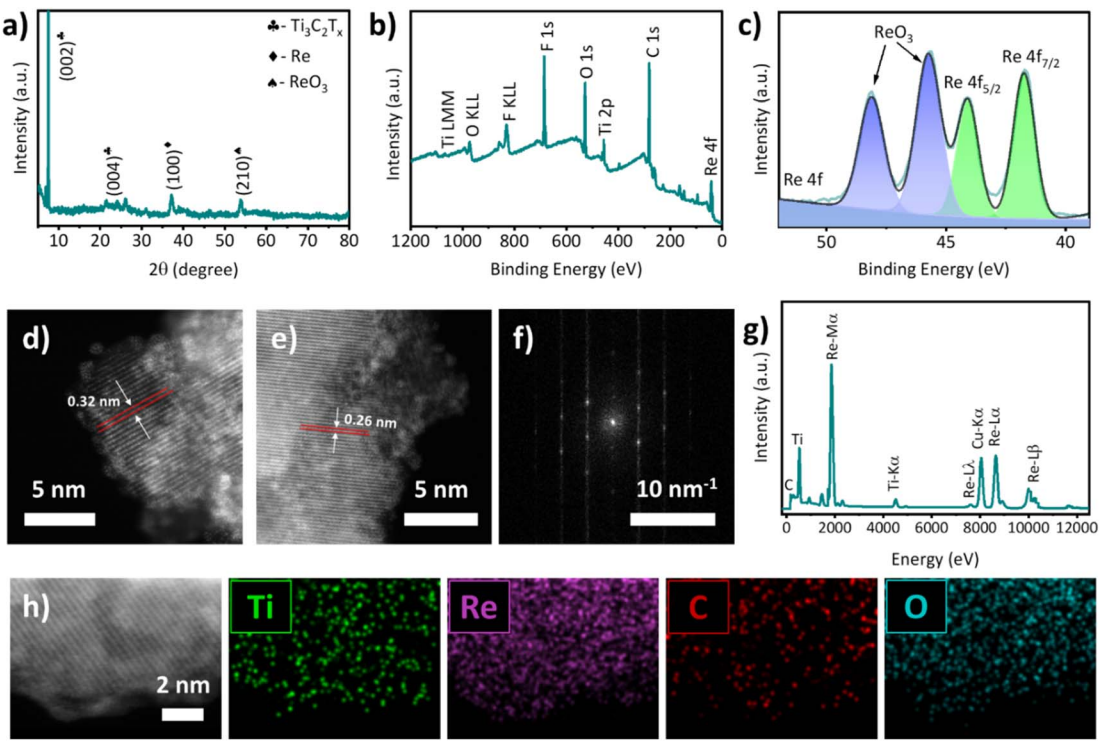

Fig. 2 (a) XRD pattern, (b) XPS survey scan, (c) HR Re 4f spectra, (d and e) HRTEM images, (f) SAED pattern, (g) EDX spectrum and (h) HAADF-STEM image and the corresponding EDX elemental mapping images of Re@$Ti_3C_2T_x$.

ultrasmall (Re) nanoparticles with an excellent lattice structure are dispersed on the edge of the MXene sheets. The particle size of the Re can be measured to be 1–3 nm. As shown in Fig. 2f, the selected area electron diffraction (SAED) pattern demonstrates that our Re@$Ti_3C_2T_x$ is highly crystalline although the sample was prepared using high annealing temperatures. To extend the proof of successful preparation, the chemical composition of Re@$Ti_3C_2T_x$ was studied using EDX (Fig. 2g), and HAADF-STEM coupled with elemental mapping (Fig. 2h). As illustrated in Fig. 2g, Ti, C, Re and Cu elements were mainly detected with Cu being from the grid for TEM. This is consistent with the XPS survey scan of our Re@$Ti_3C_2T_x$. Moreover, all expected elements including Ti, Re, C and O can be observed with excellent distribution from the EDX elemental mapping images (see Fig. 2h). In addition, we carried out inductively coupled plasma-optical emission spectrometry (ICP-OES) to determine the content of both Ti and Re in the sample. The measured Ti and Re content was 299 ppm and 17.63 ppm, respectively, leading to a mass ratio of 17 : 1 (Ti : Re), which was different from the content that can be measured from the XPS analysis shown in Fig. 2b. This difference is due to the fact that XPS is an effective tool to analyze the elemental and chemical composition of the very top surface (1–10 nm) of the sample.

The electrocatalytic HER activities of the samples including $Ti_3C_2T_x$, Re@$Ti_3C_2T_x$ and Pt catalysts were studied in an acidic medium (0.5 M H_2SO_4) with a three-electrode system. Fig. 3a displays the linear scan voltammetry (LSV) curves of the catalysts obtained by applying potentials from −1 V to 0 V (*vs.* RHE, reversible hydrogen electrode). At a constant potential of 500 mV, the measured current densities reveal that Pt exhibits remarkable catalytic activity (achieved 235.1 mA cm^{-2}) while a glassy carbon (GC) electrode is inactive for the HER (Fig. S3†). Moreover, it can be seen that the pure MXene ($Ti_3C_2T_x$) showed poor catalytic performance which is in agreement with recent work.[38] Indeed, our Re@$Ti_3C_2T_x$ catalyst exhibited much improved electrocatalytic performance, achieving a current density of 81.3 mA cm^{-2} at 500 mV. This result indicates that the introduction of Re and ReO_3 significantly improves the electrocatalytic activity of the MXene for the HER. Similarly, we compared the overpotential values of GC, pure $Ti_3C_2T_x$, Re@$Ti_3C_2T_x$ and Pt to obtain 10 mA cm^{-2} (see Fig. 3b). It is well established that a current density of 10 mA cm^{-2} has become the benchmark value used to evaluate the activity of HER electrocatalysts.[39] The required potential to achieve a current density of 10 mA cm^{-2} for Re@$Ti_3C_2T_x$ was 298 mV, while the pure MXene catalyst needed a much higher potential (584 mV), demonstrating the excellent catalytic performance of Re nanoparticles (see Table S1† for comparison).

The HER kinetics of the catalysts were studied using Tafel plots obtained from the LSV curves (Fig. 3c). The Tafel slope recorded for Re@$Ti_3C_2T_x$ was calculated to be 110.8 mV dec^{-1}, which was significantly lower than that of $Ti_3C_2T_x$ (186.8 mV dec^{-1}). The lower value of Tafel slopes indicates better catalytic kinetics due to the remarkable increase in the electrocatalytic current density.[40–42] Moreover, the Tafel slope value of Re@$Ti_3C_2T_x$ was even comparable to that of the Pt catalyst (51.5 mV dec^{-1}), showing great promise as low-cost catalysts. In addition, the electrocatalytic activity of commercial Re_2O_7 was tested to demonstrate the importance of MXene as a solid support in the catalyst. As shown in Fig. 3d, the overpotential

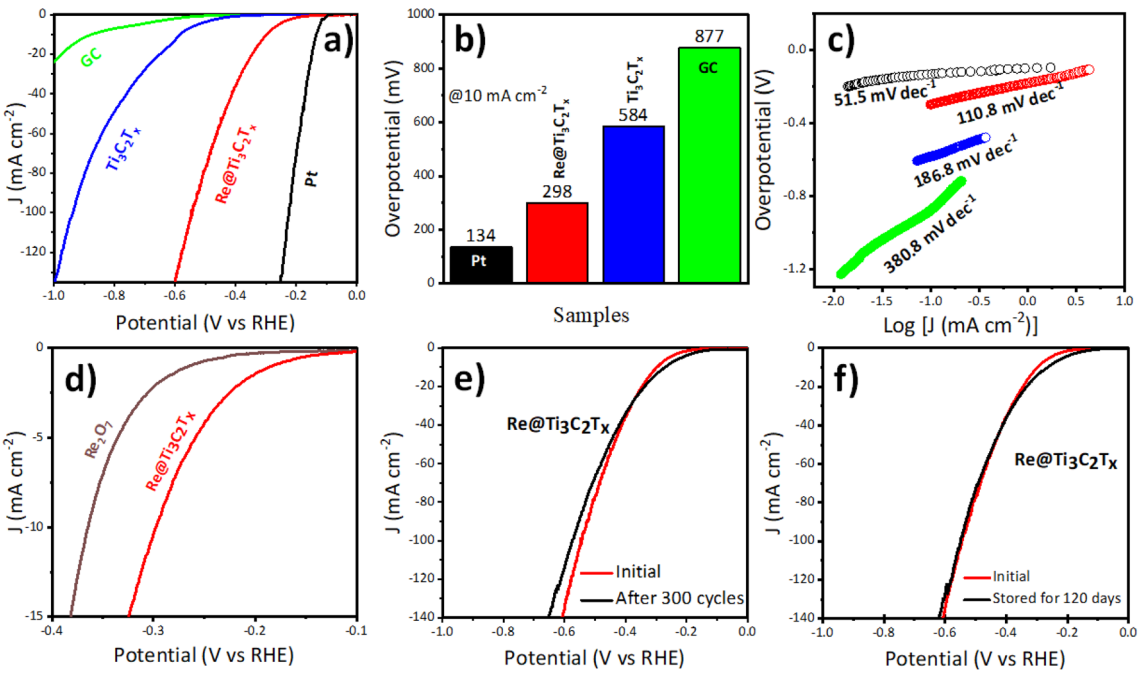

Fig. 3 (a) LSV curves, (b) overpotential values at 10 mA cm^{-2}, (c) Tafel plots of the four catalysts including GC (green), $Ti_3C_2T_x$ (blue), Re@$Ti_3C_2T_x$ (red) and Pt wire (black). (d) LSV curves of Re@$Ti_3C_2T_x$ (red) and Re_2O_7 (brown) catalysts. (e) LSV curves of Re@$Ti_3C_2T_x$ before and after 300 CV cycles. (f) LSV curves of Re@$Ti_3C_2T_x$ before and after storing in water for 120 days. Note: A Pt disk electrode was used as the control.

value of Re_2O_7 was 365 mV to reach 10 mA cm^{-2}. We further demonstrated the robustness and stability of our Re@$Ti_3C_2T_x$ under various testing conditions. As displayed in Fig. 3e, no significant changes were observed in the LSV curves of Re@$Ti_3C_2T_x$ before and after 300 continuous CV cycles. Moreover, the electrocatalytic performance of our Re@$Ti_3C_2T_x$ was well maintained in water for an extended period (120 days) (Fig. 3f), revealing that our catalyst is very stable in aqueous media. In contrast, the electrocatalytic performance of the pure MXene dramatically degraded when stored in water for only 30 days (Fig. S4†).

To understand the HER and the fundamental electronic properties of $Ti_3C_2O_2$ (MXene) in terms of Re-defects at the atomistic level, density functional theory (DFT) calculations were performed using a Vienna *Ab initio* simulation package (VASP) code[43] (see the DFT calculation details). $Ti_3C_2O_2$ was chosen for the calculations considering the O-rich termination groups on the surface of the MXene (Fig. S5†). We considered two Re-anchored MXene structures by anchoring the surface oxygen atoms of the $Ti_3C_2O_2$ slab with a single Re atom (Fig. S6a and b†) and dual Re atoms (Fig. 4a and b), respectively. We

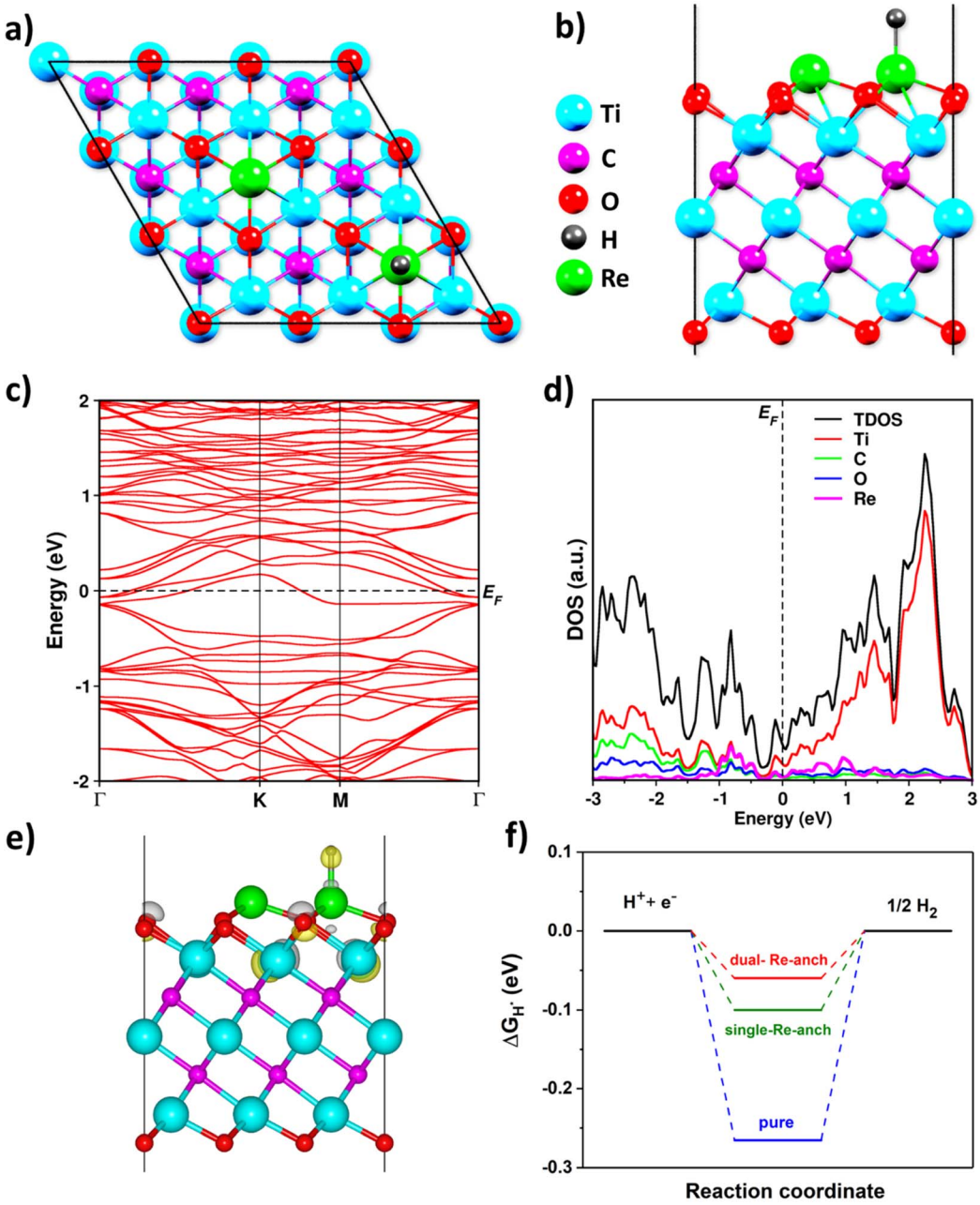

Fig. 4 (a) Top and (b) side structural views of the dual Re-anchored $Ti_3C_2O_2$. (c) The band structure and (d) DOS of the dual Re-anchored $Ti_3C_2O_2$. (e) Charge difference for H adsorption on the dual Re-anchored $Ti_3C_2O_2$, where the yellow (gray) distribution reflects the charge accumulation (depletion) in the density of 0.035*e* $bohr^{-3}$. (f) Gibbs free energy (ΔG_{H^*}) diagram of $Ti_3C_2O_2$ (pure), single Re-anchored $Ti_3C_2O_2$ (single Re-anch), and dual Re-anchored $Ti_3C_2O_2$ (dual Re-anch) for the HER at the equilibrium potential.

further discuss the dual Re-anchored $Ti_3C_2O_2$ since it shows remarkable performance.

The band structure of the dual Re-anchored $Ti_3C_2O_2$ displays the metallic feature without a bandgap (Fig. 4c), reflecting that Re-anchoring has a good impact on the electronic properties of the material. According to the density of states (DOS), Re-anchoring creates new electronic states near the Fermi level (Fig. 4d), suggesting that Re-anchored $Ti_3C_2O_2$ can to show good electronic conductivity. These features are highly supportive of the HER. Meanwhile, the charge density difference ($\Delta\rho$) in the Re-anchored $Ti_3C_2O_2$ is found not only on the H-atom and the Re-anchored O-atoms, but also on the next neighboring Ti-atoms (Fig. 4e), indicating that the surface atoms with the support of Re atoms tend to participate in the HER effectively. For H adsorption on the dual Re-anchored $Ti_3C_2O_2$, the calculated Gibbs free energy (ΔG_{H^*}) is -0.06 eV (Fig. 4f), which was $\sim$5 times better value than that of the pure one. This suggests that the Re-anchoring is favorable to improve the electrocatalytic activity of MXenes for the HER.

Conclusion

In conclusion, we have successfully synthesized $Ti_3C_2T_x$ (MXene) nanosheets as a solid support for hosting ultrasmall sized Re nanoparticles (Re@$Ti_3C_2T_x$) for enhanced hydrogen production. The catalytic activity of Re@$Ti_3C_2T_x$ is explored using a combination of experimental analysis and DFT calculations. According to our experimental investigation and theoretical calculations, Re@$Ti_3C_2T_x$ significantly improves the intermediate H* adsorption kinetics for the HER. Specifically, our newly designed Re@$Ti_3C_2T_x$ showed promising catalytic activity with a low overpotential of 298 mV to achieve 10 mA cm^{-2}, while exhibiting excellent stability over 300 continuous CV cycles and in aqueous media for 120 days. This work highlights a facile strategy for designing 2D MXene nanosheets as an efficient solid support for high performance HER electrocatalysts.

Author contributions

Selengesuren Suragtkhuu: data curation, formal analysis, investigation, methodology and writing – original draft. Suvdanchimeg Sunderiya: data curation, investigation, methodology and writing – review & editing. Solongo Purevdorj: data curation, investigation, methodology and writing – review & editing. Munkhjargal Bat-Erdene: data curation, methodology and writing – review & editing. Batjargal Sainbileg: data curation, methodology, software, validation and writing – review & editing. Michitoshi Hayashi: resources, software, validation and writing – review & editing. Abdulaziz S. R. Bati: data curation, methodology and writing – review & editing. Joseph G. Shapter: funding acquisition, resources, visualization and writing – review & editing. Sarangerel Davaasambuu: conceptualization, funding acquisition, project administration, resources, supervision, validation and writing – review & editing. Munkhbayar Batmunkh: conceptualization, funding acquisition, investigation, resources, supervision, validation and writing – review & editing.

Conflicts of interest

The authors declare no conflict of interest.

Acknowledgements

This research was supported by Fellow research grant of National University of Mongolia (P2021-4197). This work was also financially supported by the Australian Research Council (DE220100521 and DP200101217). The authors thank the research group of Dr Munkhjargal Burenjargal at the National University of Mongolia for their facility support. M. H. and B. S. are thankful to the Center of Atomic Initiative for New Materials, National Taiwan University (project No. 109L4000 and 110L9008) under the Ministry of Education of Taiwan for the funding support. A. S. R. B acknowledges support from King Abdullah University of Science and Technology (KAUST) through the Ibn Rushd Postdoctoral Fellowship Award. The authors gratefully acknowledge the use of Centre for Microscopy and Microanalysis (CMM) facilities at the University of Queensland, Australia.

References

1 Z. Chen, X. Duan, W. Wei, S. Wang and B.-J. Ni, *J. Mater. Chem. A*, 2019, **7**, 14971–15005.
2 J. Zhu, L. Hu, P. Zhao, L. Y. S. Lee and K.-Y. Wong, *Chem. Rev.*, 2020, **120**, 851–918.
3 X. Zou and Y. Zhang, *Chem. Soc. Rev.*, 2015, **44**, 5148–5180.
4 L. Yuekun, L. Li, L. Fangyan, W. Biao, G. Feng, L. Chuan, F. Jingyun, H. Feng, L. Zhang and W. Mengye, *Nano Res.*, 2022, **15**, 7986–7993.
5 J. N. Hansen, H. Prats, K. K. Toudahl, N. Mørch Secher, K. Chan, J. Kibsgaard and I. Chorkendorff, *ACS Energy Lett.*, 2021, **6**, 1175–1180.
6 Y. Guo, T. Park, J. W. Yi, J. Henzie, J. Kim, Z. Wang, B. Jiang, Y. Bando, Y. Sugahara, J. Tang and Y. Yamauchi, *Adv. Mater.*, 2019, **31**, 1807134.
7 A. S. R. Bati, M. Batmunkh and J. G. Shapter, *Adv. Energy Mater.*, 2020, **10**, 1902253.
8 Y. Li, H. Wang, L. Xie, Y. Liang, G. Hong and H. Dai, *J. Am. Chem. Soc.*, 2011, **133**, 7296–7299.
9 S. Suragtkhuu, M. Bat-Erdene, A. S. R. Bati, J. G. Shapter, S. Davaasambuu and M. Batmunkh, *J. Mater. Chem. A*, 2020, **8**, 20446–20452.
10 P. Sriram, A. Manikandan, F.-C. Chuang and Y.-L. Chueh, *Small*, 2020, **16**, 1904271.
11 M. Naguib, M. Kurtoglu, V. Presser, J. Lu, J. Niu, M. Heon, L. Hultman, Y. Gogotsi and M. W. Barsoum, *Adv. Mater.*, 2011, **23**, 4248–4253.
12 C. Wang, S. Chen and L. Song, *Adv. Funct. Mater.*, 2020, **30**, 2000869.
13 A. Lipatov, M. Alhabeb, M. R. Lukatskaya, A. Boson, Y. Gogotsi and A. Sinitskii, *Adv. Electron. Mater.*, 2016, **2**, 1600255.
14 M. Ghidiu, M. R. Lukatskaya, M.-Q. Zhao, Y. Gogotsi and M. W. Barsoum, *Nature*, 2014, **516**, 78–81.

15 X. Li, Z. Huang, C. E. Shuck, G. Liang, Y. Gogotsi and C. Zhi, *Nat. Rev. Chem.*, 2022, **6**, 389–404.
16 L. Guojin, L. Xinliang, W. Yanbo, Y. Shuo, H. Zhaodong, Y. Qi, W. Donghong, D. Binbin, Z. Minshen and Z. Chunyi, *Nano Res. Energy*, 2022, **1**, e9120002.
17 J. Zhou, X. Zha, X. Zhou, F. Chen, G. Gao, S. Wang, C. Shen, T. Chen, C. Zhi, P. Eklund, S. Du, J. Xue, W. Shi, Z. Chai and Q. Huang, *ACS Nano*, 2017, **11**, 3841–3850.
18 G. Xin, W. Changda, W. Wenjie, Z. Quan, X. Wenjie, Z. Pengjun, W. Shiqiang, C. Yuyang, Z. Kefu, L. Zhanfeng, Y. Xiya, W. Yixiu, W. Xiaojun, S. Li, C. Shuangming and L. Xiaosong, *Nano Res. Energy*, 2022, **1**, e9120026.
19 A. Agresti, A. Pazniak, S. Pescetelli, A. Di Vito, D. Rossi, A. Pecchia, M. Auf der Maur, A. Liedl, R. Larciprete, D. V. Kuznetsov, D. Saranin and A. Di Carlo, *Nat. Mater.*, 2019, **18**, 1228–1234.
20 M. R. Lukatskaya, O. Mashtalir, C. E. Ren, Y. Dall'Agnese, P. Rozier, P. L. Taberna, M. Naguib, P. Simon, M. W. Barsoum and Y. Gogotsi, *Science*, 2013, **341**, 1502–1505.
21 X. Zhang, Z. Zhang, J. Li, X. Zhao, D. Wu and Z. Zhou, *J. Mater. Chem. A*, 2017, **5**, 12899–12903.
22 M. Bat-Erdene, M. Batmunkh, B. Sainbileg, M. Hayashi, A. S. R. Bati, J. Qin, H. Zhao, Y. L. Zhong and J. G. Shapter, *Small*, 2021, **17**, 2102218.
23 Z. W. Seh, K. D. Fredrickson, B. Anasori, J. Kibsgaard, A. L. Strickler, M. R. Lukatskaya, Y. Gogotsi, T. F. Jaramillo and A. Vojvodic, *ACS Energy Lett.*, 2016, **1**, 589–594.
24 S.-Y. Bae, J. Mahmood, I.-Y. Jeon and J.-B. Baek, *Nanoscale Horiz.*, 2020, **5**, 43–56.
25 J. Zhang, Y. Zhao, X. Guo, C. Chen, C.-L. Dong, R.-S. Liu, C.-P. Han, Y. Li, Y. Gogotsi and G. Wang, *Nat. Catal.*, 2018, **1**, 985–992.
26 M. Cabán-Acevedo, M. L. Stone, J. R. Schmidt, J. G. Thomas, Q. Ding, H. C. Chang, M. L. Tsai, J. H. He and S. Jin, *Nat. Mater.*, 2015, **14**, 1245–1251.
27 J. Mahmood, F. Li, S. M. Jung, M. S. Okyay, I. Ahmad, S. J. Kim, N. Park, H. Y. Jeong and J. B. Baek, *Nat. Nanotechnol.*, 2017, **12**, 441–446.
28 T. T. Yang, R. B. Patil, J. R. McKone and W. A. Saidi, *Catal. Sci. Technol.*, 2021, **11**, 6832–6838.
29 M. Kim, Z. Yang, J. H. Park, S. M. Yoon and B. A. Grzybowski, *ACS Appl. Nano Mater.*, 2019, **2**, 2725–2733.
30 M. Alhabeb, K. Maleski, B. Anasori, P. Lelyukh, L. Clark, S. Sin and Y. Gogotsi, *Chem. Mater.*, 2017, **29**, 7633–7644.
31 L. Yu, A. S. R. Bati, T. S. L. Grace, M. Batmunkh and J. G. Shapter, *Adv. Energy Mater.*, 2019, **9**, 1901063.
32 M. Ghidiu, J. Halim, S. Kota, D. Bish, Y. Gogotsi and M. W. Barsoum, *Chem. Mater.*, 2016, **28**, 3507–3514.
33 S. Ghosh, H.-C. Lu, S. H. Cho, T. Maruvada, M. C. Price and D. J. Milliron, *J. Am. Chem. Soc.*, 2019, **141**, 16331–16343.
34 V. Urbanová, N. Antonatos, J. Plutnar, P. Lazar, J. Michalička, M. Otyepka, Z. Sofer and M. Pumera, *ACS Nano*, 2021, **15**, 2374–2385.
35 M. Zhong, S. Yan, J. Xu, C. Wang and X. Lu, *Inorg. Chem. Front.*, 2022, **9**, 4881–4891.
36 K. Zhang, M. Di, L. Fu, Y. Deng, Y. Du and N. Tang, *Carbon*, 2020, **157**, 90–96.
37 C. T. Sims, C. M. Craighead and R. I. Jaffee, *JOM*, 1955, **7**, 168–179.
38 Y. Zou, S. A. Kazemi, G. Shi, J. Liu, Y. Yang, N. M. Bedford, K. Fan, Y. Xu, H. Fu, M. Dong, M. Al-Mamun, Y. L. Zhong, H. Yin, Y. Wang, P. Liu and H. Zhao, *EcoMat*, 2022, e12274.
39 C. C. L. McCrory, S. Jung, I. M. Ferrer, S. M. Chatman, J. C. Peters and T. F. Jaramillo, *J. Am. Chem. Soc.*, 2015, **137**, 4347–4357.
40 M. Cabán-Acevedo, M. L. Stone, J. R. Schmidt, J. G. Thomas, Q. Ding, H.-C. Chang, M.-L. Tsai, J.-H. He and S. Jin, *Nat. Mater.*, 2015, **14**, 1245–1251.
41 M.-R. Gao, J.-X. Liang, Y.-R. Zheng, Y.-F. Xu, J. Jiang, Q. Gao, J. Li and S.-H. Yu, *Nat. Commun.*, 2015, **6**, 5982.
42 D. H. Kweon, M. S. Okyay, S.-J. Kim, J.-P. Jeon, H.-J. Noh, N. Park, J. Mahmood and J.-B. Baek, *Nat. Commun.*, 2020, **11**, 1278.
43 G. Kresse and J. Furthmüller, *Phys. Rev. B: Condens. Matter Mater. Phys.*, 1996, **54**, 11169–11186.